Journal of Applied Physics ARTICLE pubs.aip.org/aip/jap

Time-resolved pump–probe spectroscopic ellipsometry of cubic GaN II: Absorption edge shift with gain and temperature effects

Cite as: J. Appl. Phys. **134**, 075703 (2023); doi: 10.1063/5.0153092
Submitted: 4 April 2023 · Accepted: 29 July 2023 ·
Published Online: 17 August 2023

Elias Baron,[1,a)] Rüdiger Goldhahn,[1] Shirly Espinoza,[2] Martin Zahradník,[2] Mateusz Rebarz,[2] Jakob Andreasson,[2] Michael Deppe,[3] Donat J. As,[3] and Martin Feneberg[1]

AFFILIATIONS

[1]Institut für Physik, Otto-von-Guericke-Universität Magdeburg, Universitätsplatz 2, 39106 Magdeburg, Germany
[2]ELI Beamlines Facility, The Extreme Light Infrastructure ERIC, Za Radnicí 835, 25241 Dolní B˘re˘zany, Czech Republic
[3]Department of Physics, University of Paderborn, Warburger Straße 100, 33098 Paderborn, Germany

[a)]**Author to whom correspondence should be addressed:** elias.baron@ovgu.de

ABSTRACT

We recently published a study concerning femtosecond pump–probe absorption edge spectroscopy of cubic GaN (fundamental bandgap: 3.23 eV), resulting in the transient dielectric function. In the present study, we continue our investigations of those pump–probe measurements by determining the time-dependent transition energy at the Fermi-vector between the conduction and valence bands. The generation of electron–hole pairs by the 266 nm pump-beam (4.66 eV) shifts the absorption edge by ≈500 meV within 1 ps due to many-body effects like band-filling and bandgap renormalization. Modeling this ultra-fast change is achieved by converting the transition energies into free-carrier concentrations, assuming the electron contributions to be dominant. We consider the relaxation, recombination, and diffusion of those free-carriers as well as either an additional gain-recombination or temperature effects. This allows for describing the transition energies on short time scales. Both models yield similar values for the characteristic relaxation time (≈0.21 ps), recombination time (≈25 ps), and diffusion coefficient (≈1 cm^2/s).

I. INTRODUCTION

Although the metastable zincblende phase of the widely known GaN displays some challenges concerning growth, its intriguing properties make it a promising candidate for several modern applications like high-speed devices[1] and qubits.[2] Zincblende GaN (zb-GaN) offers a wide direct bandgap of 3.23 eV at the Γ-point of the Brillouin zone and a higher crystal symmetry than its wurtzite counterpart. Additionally, the absence of spontaneous and piezoelectric polarization in certain crystal directions[3,4] makes cubic materials promising candidate materials for closing the green-gap.[5–7] A lot of interesting research is still being performed on the various possibilities of this material.[8,9] Furthermore, recent improvements regarding the control and quality of zb-GaN have been reported.[6,10,11]

The introduction of free charge carriers, either by doping or photo-excitation, can influence the optical properties of the material.[12–16] These many-body effects change the transition energy E_{CV} between the conduction and valence band by means of bandgap renormalization (BGR) and the Burstein–Moss shift (BMS). The Fermi-energy is pushed into the respective band due to phase-space filling, which shifts the absorption edge dependent on carrier concentration. On the other hand, an optical analysis of the absorption properties, therefore, offers an insight into the free-carrier concentration within the sample. Understanding these effects is an essential step both for developing and employing novel applications.

Recently, we performed state-of-the-art optical measurements in the form of time-resolved spectroscopic ellipsometry (trSE)[17–21] on an undoped zb-GaN sample.[22] This exceptional measurement technique, based on a pump–probe approach, enables us to investigate systems under strong non-equilibrium conditions in the

femtosecond regime. Furthermore, zb-GaN is a suitable material for those investigations due to its high symmetry[23] and direct bandgap at the Γ-point of the Brillouin zone. Electron scattering[17] should also be negligible due to the absence of additional conduction band minima around the Γ-point.[24–27] Our earlier study[22] focused mainly on the determination of the time-dependent dielectric function (DF, $\varepsilon = \varepsilon_1 + i\varepsilon_2$), while considering a free-carrier profile within the sample generated by the pump-beam. The present study describes a quantitative analysis of the change of the transition energy in excited zb-GaN. The initial pump-beam absorption generates up to $4 \times 10^{20}\,\mathrm{cm}^{-3}$ electron–hole pairs at the sample surface, affecting the optical properties. Here, different processes that influence the free-carrier concentration have to be considered with many-body effects to accurately describe the temporal-evolution of the transition energy. For this, relaxation, recombination, diffusion, and an additional fast gain-recombination are considered for the free-electrons in the conduction band minimum.

II. EXPERIMENTAL

We characterize a thin film sample of zb-GaN grown by plasma-assisted molecular beam epitaxy on a 3C-SiC/Si substrate in (001) orientation. Previous studies on this exact sample revealed basic properties like layer thickness and room-temperature absorption edge,[12] as well as the time-dependent DF.[22]

Using the third harmonic of a titanium sapphire laser, trSE measurements based on a pump–probe approach were performed. The variable delay-line enabled us to obtain time-resolved transient reflectance-difference ($\Delta R/R$) data between −10 and 5000 ps with $t = 0$ representing the pump-beam incidence. The pulsed pump-beam offers 2.9 μJ at 266 nm (4.66 eV) with a 477 μm beam diameter (pump fluence: $1.62\,\mathrm{mJ/cm^2}$). The probe-beam measures the ellipsometric angles Ψ and Δ in a polarizer-sample-compensator-analyzer configuration between 1.5 and 3.7 eV. The thickness of the zb-GaN layer was determined by spectroscopic ellipsometry to be 605 nm, which is greater than the ≈60 nm characteristic absorption depth for zb-GaN at 4.66 eV.[12] Thus, a free-carrier gradient generated by the pump-beam absorption has to be considered for analyzing the measurement data. This is realized by a combination of function-based and effective medium approach grading within the WVASE32 software. A so-called point-by-point (pbp) fit, which numerically changes the DF wavelength by wavelength, reveals the DF[28,29] of the top-most (highly excited) part of the zb-GaN layer for different delay-times. Here, we approximate the inflection point of the imaginary part of the absorption onset as the transition energy at the Fermi-vector between the conduction and the valence bands.[12] A far more detailed description of the experimental setup and the analysis of the optical data can be found in our previous study.[22]

III. THEORY

Understanding the temporal development of the transition energy requires the knowledge of the free-carrier concentration within the sample as well as how these free-carriers influence the absorption edge. In this section, we approximate the free-carrier concentration in the top-most part of the zb-GaN layer and describe our necessary assumptions regarding the many-body effects that change the transition energies.

A. Free-carrier concentration

Although the pump-beam creates free-electrons in the conduction band and free holes in the valence bands, we only consider the effects of the free-electron concentration n in this study. On the one hand, it has been shown that the impact of free holes on the transition energy by many-body effects is much smaller compared to free-electrons.[13] Furthermore, since the pump-induced holes are distributed over three possible valence bands, but the pump-induced electrons all accumulate in the conduction band minimum (CBM) and the electron effective mass is smaller than the effective hole mass, the Fermi-vector k_F is determined by the electrons. Thus, the transition energy E_{CV} between conduction and valence band is dictated by the free-electron concentration. On the other hand, it is reasonable to assume that holes exhibit much lower mobility than electrons. This means that the presumed diffusion effect should be dominated by the electron contribution. Also, this should indicate that the recombination process is governed by the electrons as well since they represent the minority charge carriers in this case. This approximation, while simplified, is a necessary compromise to enable us to obtain any sort of analytical parameters at the current state.

We previously provided a model for the free-carrier concentration in the CBM, dependent on time t and position x in the sample. This model accounts for relaxation, recombination, and diffusion of those carriers.[22] However, since we determine the transition energies only for the top-most part of the excited zb-GaN layer, we set $x = 0$ resulting in

$$n_{\mathrm{model}}(t) = \frac{n_{\mathrm{relax}}(t)}{2} \times e^{\alpha^2 D t - \frac{t}{\tau_1}} \times \mathrm{erfc}\left(\sqrt{\alpha^2 D t}\right) \quad (1)$$

with

$$n_{\mathrm{relax}}(t) = \frac{N_0}{2} \times \left(\mathrm{erf}\left(\frac{t-\gamma_0}{\tau_0}\right) + 1\right). \quad (2)$$

Here, $\alpha = 1/(60\,\mathrm{nm})$ is the absorption coefficient of zb-GaN at 4.66 eV,[12] D is the electron diffusion coefficient, and τ_1 is the characteristic recombination time. Furthermore, N_0 is the total amount of generated electron–hole pairs while γ_0 and τ_0 resemble the inflection point position and characteristic time constant of the relaxation process.

B. Many-body effects

In this study, we account for two free-carrier effects that influence the transition energy. First is the BGR which decreases the fundamental bandgap E_G by electron–electron $\Delta E_{ee}(n)$ and electron–ion $\Delta E_{ei}(n)$ interactions.[16,30] The second effect is the BMS, which describes a blue shift of the absorption edge due to phase-space filling of the conduction band, which, therefore, increases the Fermi-vector $k_F(n) = (3\pi^2 n)^{\frac{1}{3}}$ and -energy, respectively.[31,32]

Describing these effects requires some assumptions about the band structure of zb-GaN. Here, we set the direct bandgap to the center of the Brillouin zone and assume isotropic bands and a scalar effective mass. The conduction band dispersion follows a $\mathbf{k} \cdot \mathbf{p}$ perturbation theory based model containing the momentum

matrix element $P = 0.724$ eV nm.[12,30,33] This parameter is also assumed to be independent of k and temperature.[34]

The renormalized bandgap can be written as[35,36]

$$E_{\mathrm{ren}}(n) = E_{\mathrm{G}} - \Delta E_{\mathrm{ee}}(n) - \Delta E_{\mathrm{ei}}(n) \tag{3}$$

with[12]

$$\begin{aligned} \Delta E_{\mathrm{ee}}(n) &= \frac{e^2 k_{\mathrm{F}}}{2\pi^2 \varepsilon_0 \varepsilon_{\mathrm{s}}} + \frac{e^2 k_{\mathrm{TF}}}{8\pi \varepsilon_0 \varepsilon_{\mathrm{s}}} \left[1 - \frac{4}{\pi} \arctan\left(\frac{k_{\mathrm{F}}}{k_{\mathrm{TF}}}\right)\right], \\ \Delta E_{\mathrm{ei}}(n) &= \frac{e^2 n}{\varepsilon_0 \varepsilon_{\mathrm{s}} a_{\mathrm{B}}^{*} k_{\mathrm{TF}}^3}, \\ k_{\mathrm{TF}} &= \sqrt{\frac{4 k_{\mathrm{F}}}{\pi a_{\mathrm{B}}^{*}}}, \quad a_{\mathrm{B}}^{*} = \frac{4\pi \varepsilon_0 \varepsilon_{\mathrm{s}} \hbar^2}{m^{*} e^2}. \end{aligned} \tag{4}$$

These expressions are analytically approximated for an n-type doped material.[16] However, in this study, the pump-beam absorption creates large free-electron and free-hole concentrations, which should lead to electron–electron, hole–hole, and electron–hole interactions. Previous investigations suggest that the hole-induced BGR is much weaker than its electronic counterpart.[13] Therefore, we approximate the effects of hole–hole and electron–hole contributions by electron–ion contribution given in Eq. (4). Introducing the renormalized bandgap in the conduction band dispersion at the Fermi-vector yields the following model for the transition energy:[12]

$$E_{\mathrm{CV}}(n) = \frac{1}{2}\left(\frac{\hbar^2 k_{\mathrm{F}}^2}{m_{\mathrm{e}}} + \frac{\hbar^2 k_{\mathrm{F}}^2}{\bar{m}_{\mathrm{h}}} + E_{\mathrm{ren}} + \sqrt{E_{\mathrm{ren}}^2 + 4P^2 k_{\mathrm{F}}^2}\right). \tag{5}$$

Here, we approximate the contributions of the three supposed valence bands as an averaged parabolic valence band with the averaged hole mass $\bar{m}_{\mathrm{h}} = 0.61\, m_{\mathrm{e}}$,[12] where m_{e} is the free-electron mass.

IV. RESULTS

In this section, we discuss the time-dependent change of the absorption onset for selected delay-times. The underlying DFs which are used to determine the transition energies E_{CV} can be found in a previous study.[22] Since the transition energies directly correspond with the free-carrier concentration, we take advantage of a highly n-type doped sample as a reference point. The optical properties of this sample were investigated and described earlier and will not be discussed here.[12] The comparison to the measurements at delay-times of 10 and 15 ps, found in Fig. 1, reveals very similar line shapes and positions of the absorption edges. This leads us to the assumption of similar free-carrier concentrations or many-body effects, respectively. The DFs display some inconsistencies below 3.2 eV, which are caused by shifted Fabry–Pérot oscillations within the excited zb-GaN layer. They will not be discussed further here as they were addressed in our previous study.[22]

Line shape fits of the DFs are performed to obtain the transition energies of the excited GaN layer ($x = 0$) for each measurement given in Ref. 22. The results are displayed in Fig. 2. Here, an initial decrease of the transition energy is observed until $t = 0.3$ ps. This could be explained by considering that the BGR is stronger

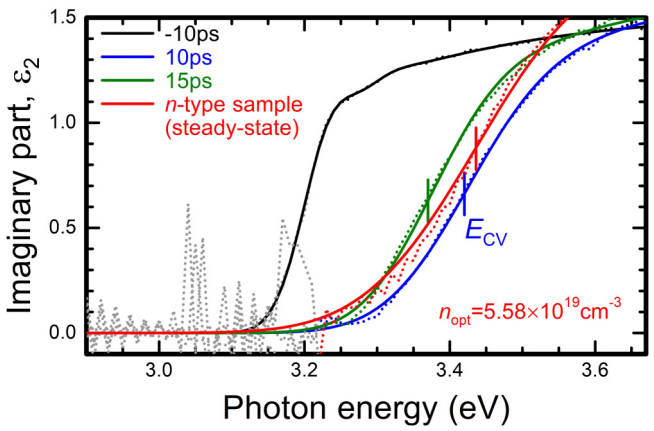

FIG. 1. Comparison of pbp- (dotted) and model- (continuous) imaginary parts of the dielectric functions between selected time-resolved measurement data of the undoped sample (10 ps, blue and 15 ps, green) and a steady-state measurement performed on an n-type zb-GaN sample (red) with an optically determined free-carrier concentration of 5.58×10^{19} cm^{-3}.[12] The steady-state result for the undoped sample is shown as well (−10 ps, black). The inflection points of the absorption onsets determine the transition energies E_{CV} (marked by vertical lines).

than the BMS for low free-carrier concentrations. A sharp increase follows, until a turning point is reached around $t = 1$ ps, at which point the relaxation is balanced by recombination and diffusion, which indicates the maximum number of free charge carriers contributing to the shift of the absorption onset. For delay-times greater than 2 ps, the transition energy steadily decreases exponentially to the steady-state case and even drops slightly below that value, again due to a stronger BGR contribution at this point, compared to the BMS.

For a better understanding of the involved processes, we convert the transition energies from Fig. 2 into free-electron concentrations at the CBM using many-body effects [Eq. (5)] and the approximations detailed in Sec. III. The results as well as a model fit, which is described later, are displayed in Fig. 3. The increase for $0.5 \leq t \leq 1.0$ ps follows

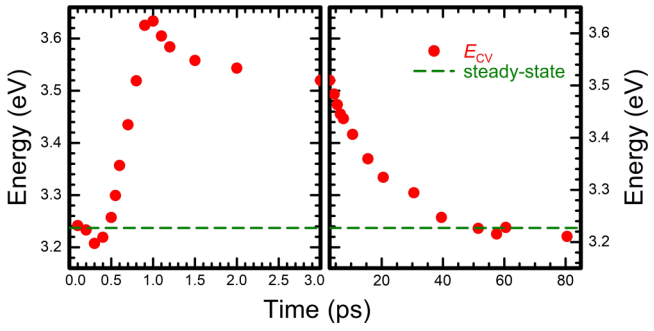

FIG. 2. Experimentally obtained transition energies E_{CV} (red dots) for different delay-times. Left: shortly after the pump-beam incidence, right: long after the pump-beam. The steady-state transition energy is indicated by the horizontal green dashed line.

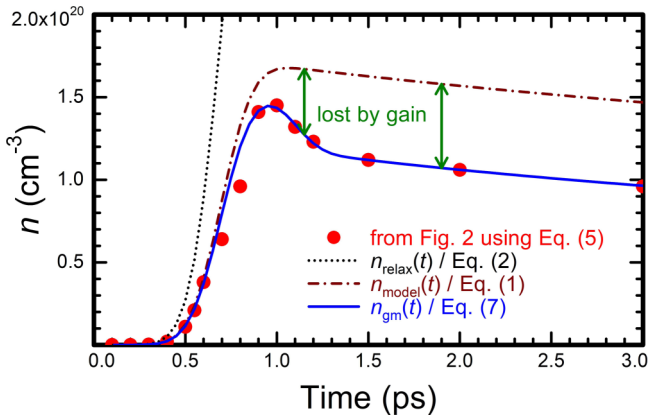

FIG. 3. Experimentally determined (red dots) and calculated (blue, continuous) free-carrier concentration in the CBM at the sample surface. Both the exclusive relaxation effect (black, dotted) and the combination of relaxation, recombination, and diffusion (brown, dashed-dotted) are displayed as well for better understanding. The difference between the blue and brown curve is explained by the loss of electron–hole pairs due to the additional gain recombination, indicated by green arrows.

the relaxation of free-carriers from the pump-reservoir. At $t \approx 1$ ps, the free-carrier concentration in the CBM strongly decreases for only 0.3 ps. We identify this fast recombination effect to be different from the recombination dominating the remaining time region until the steady-state case is reached. Compared with Ref. 22, this fast recombination process is limited to the spectra in which we included negative ε_2 contributions. Since we attribute this to material gain, we label this fast carrier reduction effect as gain-recombination. The fact that this strong decrease only takes place in a short time period suggests that this recombination process is not active the entire time but only for certain conditions. We assume the conditions to be dependent on the band-filling level. For instance, the gain-recombination only reduces the electron–hole pair concentration if the quasi-Fermi levels of both electrons and holes enter their respective bands. We model the number of electrons in the CBM lost by the gain associated recombination process as an error function,

$$n_{\mathrm{gain}}(t) = \frac{N_2}{2} \times \left(\mathrm{erf}\left(\frac{t - \gamma_2}{\tau_2} \right) + 1 \right). \tag{6}$$

Here, N_2 and τ_2 resemble the maximum number of recombined electron–hole pairs by this effect and the characteristic recombination time, respectively, while γ_2 determines the position of the inflection point of the error function. To obtain the free-carrier trend, we subtract the gain-recombination from the relaxation within Eq. (1), which yields the following revised model:

$$n_{\mathrm{gm}}(t) = \frac{\left(n_{\mathrm{relax}} - n_{\mathrm{gain}}\right)}{2} \times e^{\alpha^2 Dt - \frac{t}{\tau_1}} \times \mathrm{erfc}\left(\sqrt{\alpha^2 Dt} \right). \tag{7}$$

The model is fitted onto the determined free-carrier concentrations in Fig. 3, which results in great agreement between measurement data and theory. However, this is only for demonstrating the procedure and not for acquiring material parameters. The whole process can be described as follows: first, the pump-beam creates a large electron–hole pair concentration in a pump-reservoir, far above the band gap. These electrons and holes relax into their respective band extrema, which changes the absorption onset. Meanwhile, the quasi-Fermi levels for electrons and holes diverge. As soon as both quasi-Fermi levels enter their respective bands, the gain-related recombination process starts and thus rapidly lowers the number of electron–hole pairs.[37] Once enough electron–hole pairs have recombined so that the quasi-Fermi levels exit their bands, the fast gain-recombination stops leaving the slower recombination and diffusion processes to return the excited sample back into the steady-state case.

After successfully describing the processes that influence the free-carrier concentration in the CBM, we apply our findings to the measured transition energies in Fig. 4. Here, the model containing the gain-recombination is translated via many-body effects [Eq. (5)] into transition energies $E_{\mathrm{CV}}\left(n_{\mathrm{gm}}(t)\right)$ (blue curve in Fig. 4). The model is then fitted onto the experimental results (determined by the inflection point positions of ε_2 in our earlier study[22]). The resulting parameters for relaxation (N_0, γ_0, τ_0), recombination (τ_1), diffusion (D), and gain-recombination (N_2, γ_2, τ_2) are presented in Table I. A characteristic relaxation time of $\tau_0 = 0.19$ ps was found which is comparable with previous, theoretical estimates.[38] The obtained recombination time τ_1 is also similar to previous investigations.[39,40] Although the diffusion coefficient is considered only for electrons, the actual value is more likely to resemble an effective diffusion constant for the electron–hole plasma. The recombination time and diffusion coefficient yield a characteristic diffusion length $L_{\mathrm{D}} = \sqrt{D\tau_1} = 58.8$ nm. This is lower compared to the diffusion length found in wurtzite GaN (≈ 90 nm).[41,42]

Nevertheless, a different approach for considering the strong decrease of the transition energy can be made. Up until now, we supposed the sample to be at room-temperature. However, it is reasonable to assume that the pump-beam heats the affected area of

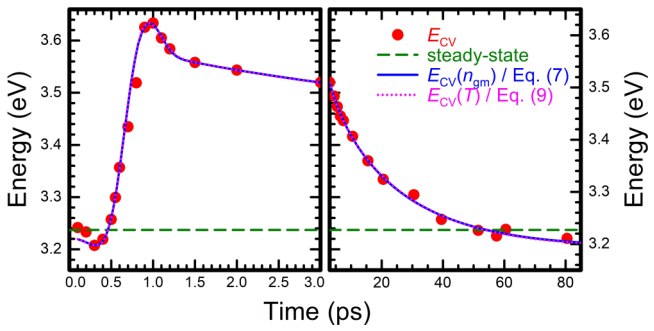

FIG. 4. Experimentally obtained (red dots) and calculated transition energies at the sample surface for different time scales. There is no significant difference between the gain-recombination model (blue continuous) and temperature effects (pink dotted). The steady-state transition energy is indicated by the horizontal green dashed line for comparison. Left: shortly after the pump-beam incidence, right: long after the pump-beam.

TABLE I. Parameters of the relaxation (Relax., N_0, γ_0, τ_0), recombination (Recom., τ_1), diffusion (Diff., D), and gain-recombination (Gain, N_2, γ_2, τ_2) contributions for the free-carrier model in Eq. (7) obtained by the best fit on the determined transition energies in Fig. 4.

	Relax. ($i = 0$)	Recom. ($i = 1$)	Diff.	Gain ($i = 2$)
N_i (cm^{-3})	3.8×10^{20}	…	…	8.1×10^{19}
γ_i (ps)	0.70	…	…	1.10
τ_i (ps)	0.19	26.1	…	0.16
D (cm^2/s)	…	…	1.33	…

TABLE II. Best fit parameters of the relaxation (Relax., N_0, γ_0, τ_0), recombination (Recom., τ_1), diffusion (Diff., D), heating (Heat., T_{high}, γ_3, τ_3), and cooling back to room-temperature (Cool., τ_4) contributions for the transition energy model in Eq. (9).

	Relax. ($i = 0$)	Recom. ($i = 1$)	Diff.	Heat. ($i = 3$)	Cool. ($i = 4$)
N_i (cm^{-3})	4.0×10^{20}	…	…	…	…
γ_i (ps)	0.74	…	…	1.09	…
τ_i (ps)	0.23	23.6	…	0.23	19.1
D (cm^2/s)	…	…	0.76	…	…
T_{high} (K)	…	…	…	544	…

the sample. The electron relaxation process is a thermalization via electron–phonon interactions. The generated phonons increase the lattice temperature of the GaN layer by phonon–phonon and phonon–electron interaction with bound electrons. This increased sample temperature reduces the fundamental bandgap of the material.[43–45] The heating rate should be directly proportional to the electron relaxation process. Therefore, we approximate the increase in surface temperature by a time-dependent function with the same characteristic behavior as the relaxation process. Cooling back to room-temperature is then assumed to be exponential. Consequently, the time-dependent temperature model results to

$$T(t) = \frac{(T_{high} - T_0)}{2} \times e^{-\frac{t}{\tau_4}} \times \left(\mathrm{erf}\left(\frac{t - \gamma_3}{\tau_3} \right) + 1 \right) + T_0, \quad (8)$$

with room-temperature $T_0 = 300$ K and the maximum temperature T_{high}. The exponential cooling is described by τ_4, while γ_3 and τ_3 resemble the inflection point position and the characteristic heating time of the error function. We set $\tau_3 = \tau_0$. However, γ_3 can and should be different from γ_0 because a delay between phonon creation through electron relaxation and bandgap reduction by phonon–phonon and phonon–electron interaction seems reasonable.

The fundamental bandgap as a function of temperature $E_G(T(t))$ is estimated by an extrapolation of the semi-empirical model introduced by Pässler.[46] The necessary parameters for zb-GaN have been reported earlier.[26] This temperature dependent bandgap is introduced in the BGR calculation in Eq. (3). However, in this study, we keep effective masses and the momentum matrix element P constant, i.e., independent on temperature. The transition energy in Eq. (5) can now be described by applying the free-carrier model from Eq. (1) and the temperature change in Eq. (8) as

$$E_{CV}(t) = E_{CV}(T(t), n_{model}(t)). \quad (9)$$

This model transition energy is now fitted onto the experimental data from Fig. 2. The fit-result is also shown in Fig. 4. Here, a good agreement between model and measurement data is achieved and no significant difference between the temperature approach and the inclusion of gain-recombination is visible. The resulting parameters for the temperature model are gathered in Table II. Fortunately, the values for relaxation, recombination and diffusion did not change dramatically compared to the alternative set of results (Table I). However, this means that we cannot differentiate between the possible gain-recombination or a temperature increase. On one hand, the temperature increase through optical pumping must occur and, therefore, has to be considered. On the other hand, the measured imaginary part of the DF displays gain effects, which cannot be described solely by temperature increase. The fact that we are able to model the behavior of the transition energy exclusively using gain-recombination or temperature increase suggests that both effects contribute to the measured ultrafast change of the absorption onset. The observed heating and cooling within ≈60 ps seems reasonable, considering the lifetime of LO phonons in wurtzite GaN was reported to be around 2 ps.[47]

V. SUMMARY

We investigated the time-dependent transition energies between the conduction and valence band of cubic GaN grown by molecular beam epitaxy on a 3C-SiC/Si (001) substrate. Time-resolved spectroscopic ellipsometry measurements between −10 and 5000 ps were performed via a pump–probe approach by a 266 nm pump-beam with a pump fluence of 1.62 mJ/cm^2. The absorption of this pump-beam generated electron–hole pairs, which influence the transition energy due to many-body interactions like bandgap renormalization and the Burstein–Moss shift. In this study, we considered only the effects of the free-electrons in the conduction band minimum. These are affected by relaxation, recombination, and diffusion processes. Analyzing the temporal development of the transition energy also revealed an additional fast gain-recombination process, which is only active for a specific time region. By applying a model for the free-carrier concentration to the measurement data, we were able to determine characteristic relaxation and recombination times as well as an effective diffusion coefficient for the free-electrons. Alternatively, the change of the transition energy could be explained by considering heating of the sample. It is our presumption that a mixture of both gain-recombination and heating (in combination with the previously mentioned effects) influence the absorption onset in cubic GaN after a high power pump-beam excitation.

ACKNOWLEDGMENTS

We gratefully acknowledge support by the Deutsche Forschungsgemeinschaft in the framework of Major Research Instrumentation Program No. INST 272/230-1 and via Project B02

within the Transregio program TRR 142 Project No. 231447078. We further acknowledge ELI Beamlines in Dolní Břežany, Czech Republic, for providing beamtime and thank the instrument group and facility staff for their assistance. This work was supported by Projects ADONIS (No. CZ.02.1.01/0.0/0.0/16-019/0000789) and ELIBIO (No. CZ.02.1.01/0.0/0.0/15-003/0000447) from the European Regional Development Fund, and by the project LM2018141 from the Czech Ministry of Education, Youth and Sport. We are thankful to Adam Nolte (Rose-Hulman Institute of Technology) for critical reading of this manuscript.

AUTHOR DECLARATIONS

Conflict of Interest

The authors have no conflicts to disclose.

Author Contributions

Elias Baron: Conceptualization (lead); Formal analysis (lead); Investigation (equal); Methodology (lead); Visualization (lead); Writing – original draft (lead); Writing – review & editing (equal). **Rüdiger Goldhahn:** Supervision (equal); Writing – original draft (equal); Writing – review & editing (equal). **Shirly Espinoza:** Data curation (equal); Investigation (equal); Resources (equal); Writing – original draft (equal); Writing – review & editing (equal). **Martin Zahradník:** Data curation (equal); Investigation (equal); Resources (equal); Writing – original draft (equal); Writing – review & editing (equal). **Mateusz Rebarz:** Investigation (equal); Resources (equal); Writing – original draft (equal); Writing – review & editing (equal). **Jakob Andreasson:** Supervision (equal); Writing – original draft (equal); Writing – review & editing (equal). **Michael Deppe:** Resources (equal). **Donat J. As:** Resources (equal); Writing – original draft (equal); Writing – review & editing (equal). **Martin Feneberg:** Conceptualization (equal); Formal analysis (equal); Project administration (equal); Writing – original draft (equal); Writing – review & editing (equal).

DATA AVAILABILITY

Raw data were generated at ELI Beamlines. Derived data supporting the findings of this study are available from the corresponding author upon reasonable request.

REFERENCES

[1]F. Schwierz, M. Kittler, H. Foster, and D. Schipanski, Diamond Relat. Mater. **6**, 1512 (1997).
[2]R. Gao, G. Bian, H. Yuan, and H. Wang, J. Phys. D: Appl. Phys. **54**, 505109 (2021).
[3]S. Li, L. Shunfeng, J. Schörmann, D. J. As, and K. Lischka, Appl. Phys. Lett. **90**, 071903 (2007).
[4]M. T. Durniak, A. S. Bross, D. Elsaesser, A. Chaudhuri, M. L. Smith, A. A. Allerman, S. C. Lee, R. J. Brueck, and C. Wetzel, Adv. Electron. Mater. **2**, 1500327 (2016).
[5]M. R. Krames, O. B. Shchekin, R. Mueller-Mach, G. O. Mueller, L. Zhou, G. Harbers, and M. G. Craford, J. Disp. Technol. **3**, 160 (2007).
[6]L. Y. Lee, Mater. Sci. Technol. **33**, 1570 (2017).
[7]B. Ding, M. Frentrup, S. M. Fairclough, G. Kusch, M. J. Kappers, D. J. Wallis, and R. A. Oliver, J. Appl. Phys. **130**, 115705 (2021).
[8]N. K. Wessling, S. Ghosh, B. Guilhabert, M. Kappers, A. M. Hinz, M. Toon, R. A. Oliver, M. D. Dawson, and M. J. Strain, Opt. Mater. Express **12**, 4606 (2022).
[9]S. Ghosh, A. M. Hinz, M. Frentrup, S. Alam, D. J. Wallis, and R. A. Oliver, Semicond. Sci. Technol. **38**, 044001 (2023).
[10]R. Liu, R. Schaller, C. Q. Chen, and C. Bayram, ACS Photonics **5**, 955 (2018).
[11]L. Y. Lee, M. Frentrup, M. J. Kappers, R. A. Oliver, C. J. Humphreys, and D. J. Wallis, J. Appl. Phys. **124**, 105302 (2018).
[12]E. Baron, R. Goldhahn, M. Deppe, D. J. As, and M. Feneberg, Phys. Rev. Mater. **3**, 104603 (2019).
[13]C. Persson, B. E. Sernelius, A. Ferreira da Silva, C. Moysés Araújo, R. Ahuja, and B. Johansson, J. Appl. Phys. **92**, 3207 (2002).
[14]M. Yoshikawa, M. Kunzer, J. Wagner, H. Obloh, P. Schlotter, R. Schmidt, N. Herres, and U. Kaufmann, J. Appl. Phys. **86**, 4400 (1999).
[15]M. Feneberg, S. Osterburg, K. Lange, C. Lidig, B. Garke, R. Goldhahn, E. Richter, C. Netzel, M. D. Neumann, N. Esser, S. Fritze, H. Witte, J. Bläsing, A. Dadgar, and A. Krost, Phys. Rev. B **90**, 075203 (2014).
[16]K.-F. Berggren and B. E. Sernelius, Phys. Rev. B **24**, 1971 (1981).
[17]S. Espinoza, S. Richter, M. Rebarz, O. Herrfurth, R. Schmidt-Grund, J. Andreasson, and S. Zollner, Appl. Phys. Lett. **115**, 052105 (2019).
[18]S. Richter, O. Herrfurth, S. Espinoza, M. Rebarz, M. Kloz, J. A. Leveillee, A. Schleife, S. Zollner, M. Grundmann, J. Andreasson, and R. Schmidt-Grund, New J. Phys. **22**, 083066 (2020).
[19]S. Richter, M. Rebarz, O. Herrfurth, S. Espinoza, R. Schmidt-Grund, and J. Andreasson, Rev. Sci. Instrum. **92**, 033104 (2021).
[20]O. Herrfurth, S. Richter, M. Rebarz, S. Espinoza, J. Zúñiga-Pérez, C. Deparis, J. Leveillee, A. Schleife, M. Grundmann, J. Andreasson, and R. Schmidt-Grund, Phys. Rev. Res. **3**, 013246 (2021).
[21]M. Zahradník, M. Kiaba, S. Espinoza, M. Rebarz, J. Andreasson, O. Caha, F. Abadizaman, D. Munzar, and A. Dubroka, Phys. Rev. B **105**, 235113 (2022).
[22]E. Baron, R. Goldhahn, S. Espinoza, M. Zahradník, M. Rebarz, J. Andreasson, M. Deppe, D. J. As, and M. Feneberg, Phys. Rev. B. (published online 2023).
[23]M. Feneberg, M. Winkler, K. Lange, M. Wieneke, H. Witte, A. Dadgar, and R. Goldhahn, Appl. Phys. Express **11**, 101001 (2018).
[24]P. Rinke, M. Winkelnkemper, A. Qteish, D. Bimberg, J. Neugebauer, and M. Scheffler, Phys. Rev. B **77**, 075202 (2008).
[25]L. C. de Carvalho, A. Schleife, and F. Bechstedt, Phys. Rev. B **84**, 195105 (2011).
[26]M. Feneberg, M. Röppischer, C. Cobet, N. Esser, J. Schörmann, T. Schupp, D. J. As, F. Hörich, J. Bläsing, A. Krost, and R. Goldhahn, Phys. Rev. B **85**, 155207 (2012).
[27]T. Lei, T. D. Moustakas, R. J. Graham, Y. He, and S. J. Berkowitz, J. Appl. Phys. **71**, 4933 (1992).
[28]D. Schmidt and M. Schubert, J. Appl. Phys. **114**, 083510 (2013).
[29]M.-Y. Xie, M. Schubert, J. Lu, P. O. A. Persson, V. Stanishev, C. L. Hsiao, L. C. Chen, W. J. Schaff, and V. Darakchieva, Phys. Rev. B **90**, 195306 (2014).
[30]J. Wu, W. Walukiewicz, W. Shan, K. M. Yu, J. W. Ager III, E. E. Haller, H. Lu, and W. J. Schaff, Phys. Rev. B **66**, 201403(R) (2002).
[31]T. S. Moss, Proc. Phys. Soc. B **67**, 775 (1954).
[32]E. Burstein, Phys. Rev. **93**, 632 (1954).
[33]E. O. Kane, J. Phys. Chem. Solids **1**, 249 (1957).
[34]P. Y. Yu and M. Cardona, *Fundamentals of Semiconductors: Physics and Materials Properties*, 4th ed. (Springer, Berlin, 2010), p. 260.
[35]M. Feneberg, J. Nixdorf, C. Lidig, R. Goldhahn, Z. Galazka, O. Bierwagen, and J. S. Speck, Phys. Rev. B **93**, 045203 (2016).
[36]R. A. Abram, G. J. Rees, and B. L. H. Wilson, Adv. Phys. **27**, 799 (1978).
[37]L. A. Coldren and S. W. Corzine, *Diode Lasers and Photonic Integrated Circuits* (Wiley, NewYork, 1995), p. 115.
[38]C. G. Rodrigues, V. N. Freire, J. A. P. da Costa, A. R. Vasconcellos, and R. Luzzi, Phys. Status Solidi B **216**, 35 (1999).
[39]R. Klann, O. Brandt, H. Yang, H. T. Grahn, and K. H. Ploog, Appl. Phys. Lett. **70**, 1808 (1997).

[40]J. H. Buß, T. Schupp, D. J. As, D. Hägele, and J. Rudolph, J. Appl. Phys. **126**, 153901 (2019).
[41]S. Hafiz, F. Zhang, M. Monavarian, V. Avrutin, H. Morkoç, Ü. Özgür, S. Metzner, F. Bertram, J. Christen, and B. Gil, J. Appl. Phys. **117**, 013106 (2015).
[42]M. Hocker, P. Maier, L. Jerg, I. Tischer, G. Neusser, C. Kranz, M. Pristovsek, C. J. Humphreys, R. A. R. Leute, D. Heinz, O. Rettig, F. Scholz, and K. Thonke, J. Appl. Phys. **120**, 085703 (2016).
[43]J. Petalas, S. Logothetidis, S. Boultadakis, M. Alouani, and J. M. Wills, Phys. Rev. B **52**, 8082 (1995).
[44]A. R. Degheidy and E. B. Elkenany, Semiconductors **45**, 1251 (2011).
[45]H. Kawai, K. Yamashita, E. Cannuccia, and A. Marini, Phys. Rev. B **89**, 085202 (2014).
[46]R. Pässler, Phys. Rev. B **66**, 085201 (2002).
[47]B. K. Ridley, J. Phys.: Condens. Matter **8**, L511 (1996).